PLOS COMPUTATIONAL BIOLOGY

RESEARCH ARTICLE

Kinetic modeling of H_2O_2 dynamics in the mitochondria of HeLa cells

Kassi T. Stein[1], **Sun Jin Moon**[1], **Athena N. Nguyen**[2], **Hadley D. Sikes**[1]*

1 Department of Chemical Engineering, Massachusetts Institute of Technology, Cambridge, MA, United States of America, **2** Department of Biological Engineering, Massachusetts Institute of Technology, Cambridge, MA, United States of America

* sikes@mit.edu

OPEN ACCESS

Citation: Stein KT, Moon SJ, Nguyen AN, Sikes HD (2020) Kinetic modeling of H_2O_2 dynamics in the mitochondria of HeLa cells. PLoS Comput Biol 16(9): e1008202. https://doi.org/10.1371/journal.pcbi.1008202

Editor: Jason M. Held, Washington University School of Medicine, UNITED STATES

Received: April 20, 2019

Accepted: July 28, 2020

Published: September 14, 2020

Data Availability Statement: All relevant data are within the manuscript and its Supporting Information files.

Funding: A GRFP Award to KTS, support from MIT's UROP office to ANN, a Samsung fellowship to SJM, and a grant from the J.H. and E.V. Wade Fund at MIT to HDS supported this work. The funders had no role in study design, data collection and analysis, decision to publish, or preparation of the manuscript.

Competing interests: The authors have declared that no competing interests exist.

Abstract

Hydrogen peroxide (H_2O_2) promotes a range of phenotypes depending on its intracellular concentration and dosing kinetics, including cell death. While this qualitative relationship has been well established, the quantitative and mechanistic aspects of H_2O_2 signaling are still being elucidated. Mitochondria, a putative source of intracellular H_2O_2, have recently been demonstrated to be particularly vulnerable to localized H_2O_2 perturbations, eliciting a dramatic cell death response in comparison to similar cytosolic perturbations. We sought to improve our dynamic and mechanistic understanding of the mitochondrial H_2O_2 reaction network in HeLa cells by creating a kinetic model of this system and using it to explore basal and perturbed conditions. The model uses the most current quantitative proteomic and kinetic data available to predict reaction rates and steady-state concentrations of H_2O_2 and its reaction partners within individual mitochondria. Time scales ranging from milliseconds to one hour were simulated. We predict that basal, steady-state mitochondrial H_2O_2 will be in the low nM range (2–4 nM) and will be inversely dependent on the total pool of peroxiredoxin-3 (Prx3). Neglecting efflux of H_2O_2 to the cytosol, the mitochondrial reaction network is expected to control perturbations well up to H_2O_2 generation rates ~50 μM/s (0.25 nmol/mg-protein/s), above which point the Prx3 system would be expected to collapse. Comparison of these results with redox Western blots of Prx3 and Prx2 oxidation states demonstrated reasonable trend agreement at short times ($\leq$ 15 min) for a range of experimentally perturbed H_2O_2 generation rates. At longer times, substantial efflux of H_2O_2 from the mitochondria to the cytosol was evidenced by peroxiredoxin-2 (Prx2) oxidation, and Prx3 collapse was not observed. A refined model using Monte Carlo parameter sampling was used to explore rates of H_2O_2 efflux that could reconcile model predictions of Prx3 oxidation states with the experimental observations.

Author summary

Cancer is a complex disease that caused the deaths of over 9 million people worldwide in 2018, according to the WHO. While great strides have been made in treating many cancers, effective chemotherapies still carry difficult side effects, motivating the search for

more targeted and selective treatments that act minimally in healthy cells. The Selective Cancer Killing Hypothesis is based on the idea that some cancers exist at endogenous levels of reactive oxygen species that are higher than healthy cells, so if a patient were systemically treated with a redox-based chemotherapeutic that raises all cells' levels of reactive oxygen species, only the cancer cells would cross a toxicity threshold. This hypothesis is attractive because it would minimize side effects in healthy cells, but the quantitative knowledge of endogenous oxidant concentrations that would be helpful in refining and testing this hypothesis is not widely established. Our model predicts the range of relevant hydrogen peroxide concentrations in the mitochondria of the HeLa model cancer cell line and suggests experimental measurements of tumor cells and tissues that may be useful in quantifying steady state concentrations of this oxidant.

Introduction

Reactive oxygen species (ROS) are a class of chemical species that promote diverse phenotypes depending on intracellular concentration, localization and cumulative dose over time, spanning the gamut from homeostasis to toxicity [1,2]. Among ROS, the behavior of hydrogen peroxide (H_2O_2) most closely resembles that of a classical signaling molecule, based on the specificity of its reactions and its *in vivo* half-life [3–6]. Mitochondria are putatively a main intracellular source of H_2O_2 under basal conditions as a result of the electron transport chain (ETC) and oxidative phosphorylation (OxPhos) [2,7]. This organelle is also hypothesized to be an important site for H_2O_2-mediated signaling [8,9].

Previous work in our group has demonstrated that H_2O_2 perturbations directed to the mitochondrial matrix elicit a marked toxicity in HeLa cells, especially when contrasted against comparable perturbations delivered in the cytosol [10,11]. This toxicity was both concentration- and time-dependent, indicating the importance of a dynamic understanding of the H_2O_2 reaction network. Building upon our experimental results, we sought to further our mechanistic understanding of mitochondrial H_2O_2 kinetics by constructing a computational model of the reaction network in this organelle. Detailed molecular mechanisms that connect changes in H_2O_2 with phenotypic responses such as changes in mitochondrial morphology, mitochondrial permeability transition (MPT), and programmed cell death have not been elucidated. Since these signaling responses occur during excursions in H_2O_2 concentration from the basal steady state, we expect that establishing a quantitative range that can be connected with phenotypic responses will help inform whether particular cysteine residues are likely to become directly oxidized [12]. Existing models on mitochondrial ROS so far have largely fallen into two categories: detailed kinetic models focusing on fast-respiring cells, such as cardiac cells [13,14], or models that exclude the thioredoxin/peroxiredoxin (Trx/Prx) system [15]. Faster rates of cellular respiration [16] and differing abundances of mitochondrial proteins, which have been reported for differing tissue and cell types [17], may lead to differing steady-state H_2O_2 concentrations. The Prxs are so abundant and react with H_2O_2 with such a high second-order rate constant (10^6–10^8 $M^{-1}s^{-1}$) that this antioxidant system cannot be neglected [18,19]. Some additional modeling efforts have focused on the kinetics of species other than H_2O_2 specifically [20] or on parameter estimation [21]. To our knowledge, this model represents the first kinetic model of the mitochondrial H_2O_2 reaction network in a transformed cell line, incorporating the most recent quantitative data specific for HeLa cells.

Here, we implement this model to predict basal H_2O_2 concentrations in HeLa cell mitochondria. We also predict network behavior in response to sustained H_2O_2 perturbations,

including the degree of oxidation of four major antioxidant species present in mitochondria: Prx3, glutathione peroxidase 1 (Gpx1), Prx5, and Gpx4. The mass action kinetics of a network of 30 reactions of 28 chemical species were described using ordinary differential equations and, after parameterization with 30 rate coefficients and species concentrations, solved using MATLAB. Basal mitochondrial H_2O_2 as well as reaction network response to H_2O_2 perturbations were predicted. Modeling results were compared with experimental data from redox Western blots of the Prxs using the mitochondrially-localized H_2O_2 generator D-amino acid oxidase (mito-DAAO). HeLa cells were exposed to a range of D-alanine concentrations, a substrate for mito-DAAO, over time, and Western blots were performed on the cell lysates to observe the change in Prx3 (mitochondrial) and Prx2 (cytosolic) oxidation with the different treatments.

Methods

Model formulation: Baseline model

This model was adapted from our previously published kinetic model of the cytosolic antioxidant network, and consists of a system of first-order ordinary differential equations of the form

$$\frac{dC_i}{dt} = R_i \tag{1}$$

where C_i is the species concentration, t is time and R_i is the net reaction for that species [22]. It assumes species concentrations are homogeneous throughout the compartment. The baseline model investigates the steady state conditions in the mitochondria, where the only source of endogenous H_2O_2 is assumed to be from the ETC due to cellular respiration. For the purposes of this simulation, the rate of H_2O_2 generation due to OxPhos is assumed to be invariant.

As a first approximation, transport of H_2O_2 between mitochondria and the cytosol is neglected. Release of H_2O_2 from isolated mitochondria to the surrounding medium has been measurable, but it has not been possible to measure H_2O_2 efflux from mitochondria to the cytosol in intact cells near basal conditions, perhaps due to insufficient sensitivity of existing analytical techniques. By modeling the reaction network with the assumption that H_2O_2 efflux is small enough to be neglected and comparing with increasing experimental perturbations to the H_2O_2 generation rate, we aim to estimate H_2O_2 generation rates for which this assumption breaks down, motivating the need for a refined model that incorporates H_2O_2 efflux. The baseline model quickly reaches steady state (less than 1 s), so baseline simulations are carried out to 5 s. The stiff equation solver ode15s in MATLAB was implemented to solve the system of equations.

The main reaction systems that this model captures are the thioredoxin/peroxiredoxin/thioredoxin reductase (Trx/Prx/TR) and the glutathione/glutathione peroxidase/glutaredoxin (GSH/Gpx/Grx) networks. The Prx isoforms found in the mitochondria are Prx3 and Prx5 [23,24], which are reduced by Trx2 [25,26]. Trx2 also reduces disulfide bonds to protein dithiols [27]. Both Gpx1 and Gpx4 are found in the mitochondria, though at low concentrations in HeLa cells [28]. Grx2 is the most abundant mitochondrial Grx isoform, and is responsible for reducing S-glutathionylated proteins [29–31]. While the prior proteins are all considered mitochondrially localized, both GSH and sulfiredoxin (Srx) are generally considered cytosolic molecules that must be imported into the mitochondria [17,32–34]. The mitochondria maintain a large pool of the former, but the latter is only imported based upon a stimulus [33,34]. Catalase is not included because it is not expected to be found in the

mitochondria for most cell types, including HeLa cells [17,28,35]. A schematic representation of the reaction networks captured by this model is shown in Fig 1.

The reaction rate parameters for mass action or Michaelis-Menten kinetics in Eq. (1) were found in the peer-reviewed literature or derived from published data. The detailed calculations necessary to derive values of some parameters can be found in S1 Appendix. For any cases where mitochondria-specific values could not be located, the cytosolic equivalent was assumed. These parameters are summarized in Table 1. One difference between previously published models and this one is the treatment of Srx. Previous work [22,38] has assumed zeroth-order kinetics with respect to Srx, leading to the following rate law for hyperoxidized Prx3:

$$\frac{d[Prx3-SOOH]}{dt} = k_{hyperox}[Prx3-SOH][H_2O_2] - k_{cat}[Prx3-SOOH] \quad (2)$$

where $k_{hyperox}$ is the rate of hyperoxidation of Prx3 and k_{cat} is the turnover number reported for Srx by Chang and colleagues [38]. However, overexpression studies have clearly demonstrated an increase in reduction rate of the sulfinic acid with increased Srx concentration [39]. The form of the rate law proposed by Eq (2) fails to capture any dependence on Srx, so we propose a rate law with first-order dependence on Srx as a first approximation:

$$\frac{d[Prx3-SOOH]}{dt} = k_{hyperox}[Prx3-SOH][H_2O_2] - k'\,[Prx3-SOOH][Srx] \quad (3)$$

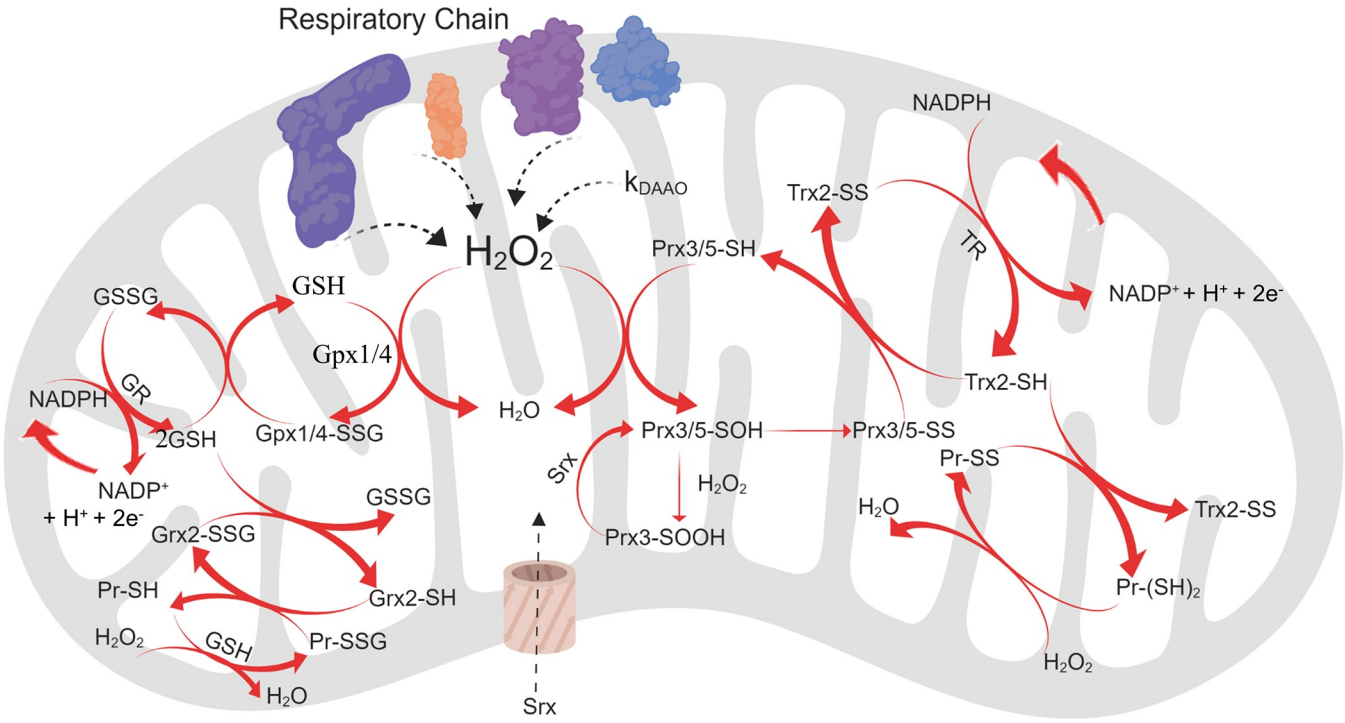

Fig 1. Schematic representation of the H_2O_2 reaction network in the mitochondria. H_2O_2 is evolved as a result of cellular respiration and the respiratory complexes at a rate that is taken as fixed for the purposes of this model. For the perturbation model only, H_2O_2 is also added to the system by a variable source term, k_{DAAO}. It can then participate in reactions with the two Prx isoforms present in the mitochondria (Prx3 and Prx5), which are reduced by Trx2. H_2O_2 can also react with either of the Gpx isoforms in the mitochondria (Gpx1 and Gpx4), which involves reduction by GSH. Both of these networks require NADPH for reduction [36,37]. Only Prx3 can undergo the hyperoxidation pathway, forming a sulfinic acid, which is reduced by Srx. Srx is imported into the mitochondria. Finally, H_2O_2 can react with protein thiols and dithiols, which are reduced by Trx2 and Grx2, respectively. Image created with Biorender.com.

https://doi.org/10.1371/journal.pcbi.1008202.g001

Table 1. Kinetic parameters. Calculations for parameters that were derived can be found in SI.

Reaction	Parameter
Generation of H_2O_2 by OxPhos	k_1 = 4 μM/s [16,40]
k_2[Gpx1red][H_2O_2]	k_2 = 60 $\mu M^{-1}s^{-1}$ [35,41]
k_3[Gpx1ox][GSH]	k_3 = 0.04 $\mu M^{-1}s^{-1}$ [42]
k_4[Gpx-SSG][GSH]	k_4 = 10 $\mu M^{-1}s^{-1}$ [42]
k_{20}[$NADP^+$]/(k_5+[$NADP^+$])	k_5 = 57 μM [43]
k_6[Prx3-SH][H_2O_2]	k_6 = 20 $\mu M^{-1}s^{-1}$ [23]
k_7[Prx3-SOH][H_2O_2]	k_7 = 0.014 $\mu M^{-1}s^{-1}$ [44]
k_8[Prx3-SOOH][Srx]	k_8 = 3x10^{-3} $\mu M^{-1}s^{-1}$ [38]
k_9[Prx3-SOH]	k_9 = 20 s^{-1} [44]
k_{10}[Prx3-SS][Trx2-SH]	k_{10} = 0.22 $\mu M^{-1}s^{-1}$ [26,45]
k_{11}[GSH]	k_{11} = 7.4x10^{-5} s^{-1} [46]
k_{12}[Pr-SH][H_2O_2]	k_{12} = 1x10^{-4} $\mu M^{-1}s^{-1}$ [47,48]
k_{13}[Pr-SOH][GSH]	k_{13} = 0.12 $\mu M^{-1}s^{-1}$ [49,50]
k_{14}[Grx2-SH][Pr-SSG]	k_{14} = 0.01 $\mu M^{-1}s^{-1}$ [51]
k_{15}[Grx2-SSG][GSH]	k_{15} = 0.04 $\mu M^{-1}s^{-1}$ [52]
k_{16}[Pr-$(SH)_2$][H_2O_2]	k_{16} = 1x10^{-4} $\mu M^{-1}s^{-1}$ [47]
k_{17}[Pr-SS][Trx2-SH]	k_{17} = 1x10^{-4} $\mu M^{-1}s^{-1}$ [47]
k_{18}[GSSG][NADPH]	k_{18} = 3.2 $\mu M^{-1}s^{-1}$ [53]
k_{19}[Trx2-SS][NADPH]	k_{19} = 20 $\mu M^{-1}s^{-1}$ [54]
k_{20}[$NADP^+$]/(k_5+[$NADP^+$])	k_{20} = 375 μM/s [43]
GSH import	k_{21} = 0.48 μM/s [55]
GSH efflux k_{22}[GSH]	k_{22} = 9.6×10^{-5} s^{-1} described in text
k_{23}[Prx5-SH][H_2O_2]	k_{23} = 0.3 $\mu M^{-1}s^{-1}$ [23,25]
k_{24}[Prx5-SOH]	k_{24} = 14.7 s^{-1} [25]
k_{25}[Prx5-SS][Trx2-SH]	k_{25} = 2 $\mu M^{-1}s^{-1}$ [25]
k_{26}[Gpx4red][H_2O_2]	k_{26} = 0.05 $\mu M^{-1}s^{-1}$ [56]
k_{27}[Gpx4ox][GSH]	k_{27} = 0.02 $\mu M^{-1}s^{-1}$ [56]
Generation of H_2O_2 by DAAO	k_{28} = k_{DAAO} described in text
Srx import	k_{29} = 1.23x10^{-5} μM/s [57]
H_2O_2 efflux	k_{30} = k_{efflux} described in text

https://doi.org/10.1371/journal.pcbi.1008202.t001

where k' is the estimated second-order rate constant, obtained by dividing 0.18 min^{-1}, the first order rate constant reported in [38], by the sulfiredoxin concentration used there. These parameters, $k_{hyperox}$ and k' correspond to k_7 and k_8 in Table 1, respectively. Glutathione efflux was treated as a first order reaction and the value was determined via trial-and-error to satisfy the constraint that the total glutathione level should not change by more than 5%, just as the total Trx level does not change over the course of the simulations in this work.

Species abundances for model initialization were either found in literature, calculated from published datasets, or calculated based on molar balances and rate laws. Species that were found in literature or calculated using published datasets are summarized in Table 2, and species that were derived from molar balances and rate laws are summarized in Table 3. Prx3-SH abundance is given as a range rather than a single value. This is the result of the calculations that are necessary to convert per-cell protein copy numbers from the proteomics dataset in [28] to a per mitochondrion concentration. For these calculations, mitochondrial volume was taken as 0.29 μm^3 [58] and mitochondrial number in a HeLa cell has been reported to range from 383–882 [59]. A total protein density throughout the cell was reported as 2x10^5 mg/L in

Table 2. Initial species abundances.

Species	Concentration (μM)
Prx3-SH	48–110 [28,58,59]
Prx5-SH	14 [28,58,59]
Gpx1	$1.5x10^{-2}$ [17,28,58,59]
Gpx4	0.23 [17,28,58,59]
Grx2	1 [28,58,59]
Trx2-SH	7.7 [28,58,59,61,62]
Trx2-SS	0.075 [63]
GSH	$5x10^{3}$ [23]
GSSG	1.78 [63]
NADPH	30 [64]
$NADP^+$	0.03 [65]
Pr-SH	$1x10^{-3}$ [47]
$Pr-(SH)_2$	$1.09x10^{3}$ [63]
Srx	$8.8x10^{-3}$ [28]

https://doi.org/10.1371/journal.pcbi.1008202.t002

[28] so we assumed this density was invariant between organelles. Additional details regarding these calculations can be found in S1 Appendix.

While all the proteins that were calculated based on the data in [28] produced a range of possible values depending on the number of mitochondria per cell, Prx3-SH was by far the most abundant and has a very high rate constant for reaction with H_2O_2. Therefore, we considered the range of Prx3-SH concentrations explicitly while taking the median value for other protein concentrations calculated from [28]. Notably, the abundances of Gpx1 and Gpx4 listed in Table 2, calculated from the proteomics dataset in [28], are much lower than values suggested in previous work with hepatocytes (2 and 1 order of magnitude lower, respectively) [60]. Because several species are initialized by molar balance, the range in Prx3-SH initialization results in several species in Table 3 to initialize differently depending on its concentration.

Table 3. Derived initial species abundances.

Species	Concentration (μM)
H_2O_2	$2x10^{-3}$ – $4x10^{-3}$
Prx3-SOH	0.18–0.20
Prx3-SS	2.2–2.3
Prx3-SOOH	0.19–0.42
Prx5-SOH	$5x10^{-4}$ – $1x10^{-3}$
Prx5-SS	$5x10^{-4}$ – $1x10^{-3}$
Gpx1ox	8x10-6 – $2x10^{-5}$
Gpx1-SSG	3x10-8 – $7x10^{-8}$
Gpx4ox	0
Gpx4-SSG	0
Grx2-SSG	$1x10^{-16}$
Pr-SOH	3x10-13 – $6x10^{-13}$
Pr-SSG	1x10-8 – $3x10^{-8}$
Pr-SS	0.26–0.59

https://doi.org/10.1371/journal.pcbi.1008202.t003

Quantifying uncertainty in model predictions

Monte Carlo parameter sampling. Based on the feasible concentration range of Prx3-SH in HeLa mitochondria, we generated 10,000 random samples (shown in S1 Appendix) spread uniformly throughout the feasible space using the following equation [66]:

$$\mathbf{C_{Prx3-SH}} = \mathbf{U(0,1)} \times [\mathbf{C^{max}_{Prx3-SH}} - \mathbf{C^{min}_{Prx3-SH}}] + \mathbf{C^{min}_{Prx3-SH}} \quad (4)$$

Here, U(0,1) refers to a single uniformly distributed random number in the range of 0 to 1, and $\mathbf{C^{min}_{Prx3-SH}}$ is 48 μM and $\mathbf{C^{max}_{Prx3-SH}}$ is 110 μM. A set of randomly generated Prx3-SH concentrations was used as initial conditions for implementation of ODE simulations, providing a distribution of predicted steady-state concentrations of each species of interest.

Sensitivity analysis. In order to calculate the sensitivity of predicted steady-state H_2O_2 concentrations and protein redox balances to the values of model parameters used, the finite difference approximation method was used [67]. The sensitivities were calculated using the following equation:

$$s_i(t) = \frac{\partial C_j(t)}{\partial k_i} = \frac{C_j(k_i + \Delta k_i, t) - C_j(k_i, t)}{\Delta k_i} \quad (5)$$

where s_i is the sensitivity corresponding to parameter k_i and C_j is the concentration of the species of interest (e.g. H_2O_2 or Prx3-SS). Parameters were perturbed by 10% to reflect an estimate of typical experimental error, and sensitivities were normalized to adjust for differences in orders of magnitude:

$$\bar{s_i}(t) = \frac{\partial C_j(t)/C_j(t)}{\partial k_i/k_i} \quad (6)$$

Sensitivities of the basal, steady-state model predictions were calculated at 5 s, and here, we report only $\bar{s_i}$.

Model formulation: H_2O_2 perturbation

The second part of this modeling endeavor sought to investigate the effects of a source of H_2O_2 perturbation, similar to what is introduced by the synthetic biology tool D-amino acid oxidase (DAAO) targeted to the mitochondrial matrix. This was modeled as a constant source term, k_{DAAO}, within the H_2O_2 rate equation, as depicted in Fig 1. Because we were interested in how the network would respond to perturbations of varying magnitudes, we swept this parameter across a range of values until we reached an upper limit of possible physiological relevance, which we defined as the complete collapse of the Prx3 system. This part of the simulation was carried out to 3600 s (1 hr).

Comparison of model predictions with experimental data

Cell culture. HeLa cells that had previously been transfected by lentivirus to stably express a mitochondrially-targeted D-amino acid oxidase (mito-DAAO) H_2O_2 generator [10] were maintained in Dulbecco's modified Eagle's medium (DMEM; Lonza), supplemented with 10% fetal bovine serum (FBS; ATCC) at 37˚C in a humidified atmosphere with 5% CO_2. Cells were passaged approximately every 3 days and were maintained under selective pressure using 6 μg/mL puromycin (Sigma) until 24 hrs before any experiments.

Analysis of Prx response to mitochondrial H_2O_2 perturbations. HeLa cells expressing mito-DAAO were seeded at $3.5x10^5$ cells/well in 6-well plates ~18 hours prior to the start of generation (target confluence ~50% at start of experiment). Cells were exposed to 5 μM flavin

adenine dinucleotide (FAD; Sigma) and concentrations of D-alanine (Sigma) from 0–25 mM in Roswell Park Memorial Institute 1640 medium (RPMI; Invitrogen) without phenol red. At the end of the H_2O_2 generation period, cells were washed with ice cold 1x phosphate buffered saline (PBS) and then incubated on ice with 2 mL 100 mM methyl methanethiosulfonate (MMTS; Sigma) for 30 min to block free thiols. Cells were washed twice more with cold PBS, then lysed in 100 μL of lysis buffer (0.5% Triton X-100 (Sigma), 1x HALT protease and phosphatase inhibitor (ThermoFisher), 1x PBS). Lysates were centrifuged on a cooled rotor for 10 min at 10,000xg and the supernatant was collected and stored at -80˚C for further analysis. Western blotting was carried out according to the protocol in [68]. Proteins were separated by non-reducing SDS-PAGE using a pre-cast 12% polyacrylamide stain-free gel (Bio-Rad). Following SDS-PAGE, the gel was activated for 45 s using a ChemiDoc MP (Bio-Rad), then proteins were transferred to a polyvinylidene difluoride (PVDF) membrane for immunoblotting. Blots were blocked using Odyssey blocking buffer (Licor), and incubated with primary antibodies against Prx3 (Abcam, ab73349), Prx2 (R&D Systems, AF3489), and Hsp60 (R&D Systems, Clone# 264233) either overnight at 4˚C or 2 hr at room temperature. Endogenous Hsp60 was used to account for differences in loading. Blots were incubated for 1 hr at room temperature with Licor IRDye secondary antibodies. The ChemiDoc MP system was used to image the blots, then ImageJ was used to quantify the images for densitometry.

Statistical analysis

Analysis of variance (ANOVA) was used to test for trends in the fractional oxidation of the Prx protein, as measured by Western blots. At least three biological replicates per time point were used for trend testing. Post-hoc Tukey's Honest Significant Difference (Tukey-HSD) testing was performed to determine which sample means were different from the control (0 mM D-ala) within each time point.

Model refinement: H_2O_2 perturbation

An H_2O_2 efflux reaction was added to represent transport of H_2O_2 out of the mitochondria and into the cytosol. Monte Carlo parameter sampling using sets of 10,000 random sample points for k_{DAAO} and k_{efflux} were generated in uncertain ranges of these parameters. For high k_{DAAO} values where efflux may be important, the minimum and maximum of k_{DAAO}, or $(k^{min}_{DAAO}, k^{max}_{DAAO})$, were set to (50, 100), where the units are μM/s. Two efflux cases were considered, termed low and high. For low k_{efflux}, $(k^{min}_{efflux}, k^{max}_{efflux})$ was set to (0, 50), and for high k_{efflux}, $(k^{min}_{efflux}, k^{max}_{efflux})$ was set to (50, 100), where the units are again μM/s. Equations following the form of (4) above together with uniformly distributed random numbers in the range of 0 to 1 were used to produce sets of parameter values, further described in S1 Appendix, that were used in implementation of ODE simulations.

Results

The first quantity investigated was the basal, steady-state concentration of H_2O_2 in mitochondria, which was predicted to range between 1.8–4.4 nM (Fig 2A). This steady-state concentration showed a strong inverse dependence on the concentration of Prx3 within a mitochondrion. Fig 2A shows that a two-fold increase in Prx3 concentration leads to a two-fold decrease in steady state H_2O_2 concentration. The range of Prx3 concentrations examined in Fig 2A reflects the current state of knowledge of this mitochondrial protein's concentration. Copy numbers of Prx3 proteins per cell have been calculated from pooled lysates of many cells [28], and number of mitochondria per cell have been measured [60], narrowing the likely

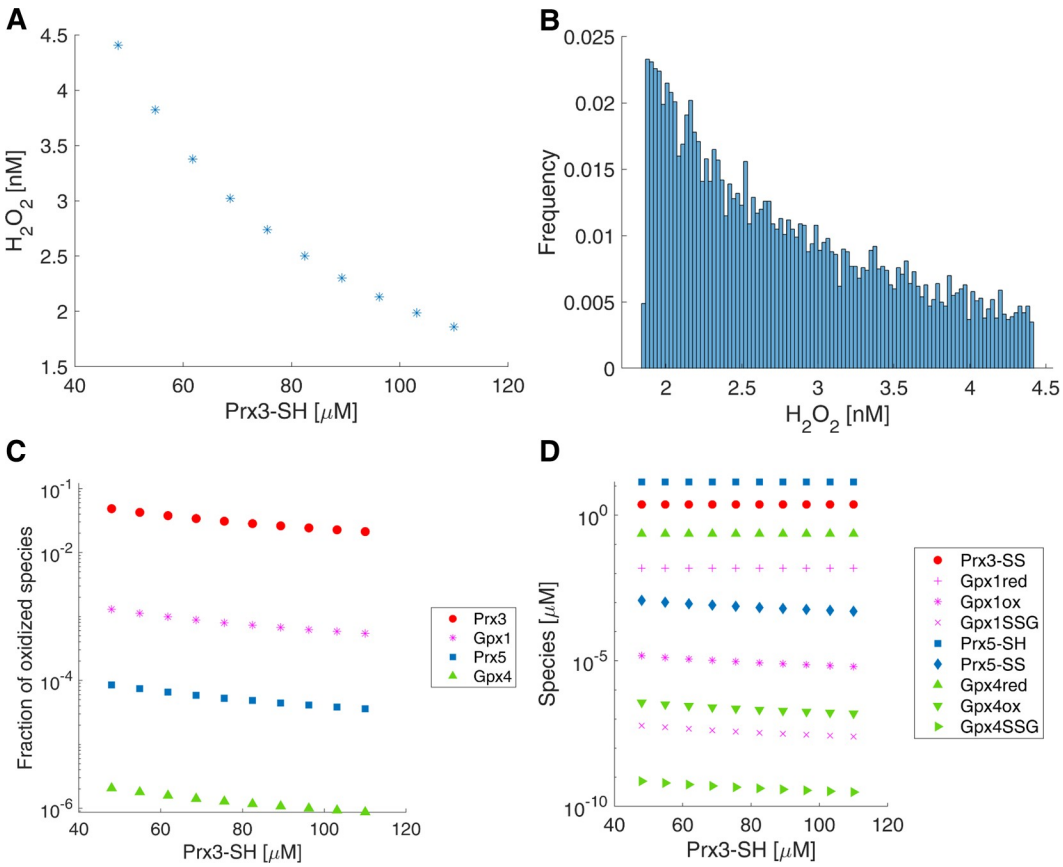

Fig 2. Baseline conditions. A) Steady state, basal [H_2O_2] in a mitochondrion with fixed H_2O_2 generation from OxPhos (4 μM/s) for different initial pools of Prx3-SH, based on possible range calculated from [28] and [60]. B) Distribution of basal [H_2O_2] based on simulation results with 10,000 randomly sampled initial Prx3-SH pools in the same range examined in A). C) Fraction of dimerized Prx3 (Prx3-SS/total Prx3), dimerized Prx5, and oxidized GPx species versus initial concentration of Prx3-SH for fixed H_2O_2 generation from OxPhos (4 μM/s). D) Steady state concentrations of oxidized and reduced forms of the four major antioxidants in the mitochondria as a function of initial Prx3-SH concentration with fixed H_2O_2 generation from OxPhos (4 μM/s). Similar plots for a fixed H_2O_2 generation rate from OxPhos of 11 μM/s can be found in S1–S3 Figs.

https://doi.org/10.1371/journal.pcbi.1008202.g002

range of Prx3 concentrations per mitochondrion, and thus basal, steady state H_2O_2 concentrations within mitochondria, to the ranges that are plotted in 2A. To supplement the ten single-point calculations presented in Fig 2A, Monte Carlo parameter sampling within the same range of Prx3 concentrations was used to further investigate the range of steady-state mitochondrial H_2O_2 concentrations, resulting in the distribution shown in Fig 2B.

We next investigated the effect of the total available pool of Prx3 on the dimer fraction of Prx3, calculated as

$$\text{fraction dimerized} = \frac{Prx3SS}{Prx3_{total}} \tag{7}$$

a quantity is often measured experimentally by Western blotting, and at baseline can characterize the variability between different cell types [10,69]. Fig 2C plots this quantity as well as the fractional oxidation of other peroxidases found within the mitochondria. Similar to the basal, steady-state H_2O_2 concentration, the fractions of oxidized peroxidases all demonstrate an inverse relationship with the total pool of Prx3. Only Prx3 experiences any significant degree of oxidation at baseline, as shown in Fig 2C and 2D and summarized in Table 4. The

fractional oxidation in Table 4 represents the dimer fraction for the Prxs and the fraction of Gpxox + GpxSSG for the Gpxs. The basal model predicts that only 2 to 5% of the total Prx3 pool is engaged in maintaining H_2O_2 at low nM concentrations, leaving a large excess of Prx3-SH.

In order to evaluate the impact that parameter uncertainties may have on the model predictions, we performed a sensitivity analysis. The value of $\bar{s_i}$ can inform us about both the magnitude and direction that changes in a particular parameter will have on the predictions for a given species of interest. For example, a sensitivity of 1 indicates that a 10% increase in the parameter resulted in a 10% increase in the model output, and likewise, a sensitivity of -1 would signify a 10% decrease in the model output. Fig 3 depicts tornado plots of the sensitivities of the predicted basal steady-state concentrations of H_2O_2 (A), Prx3-SH (B), Prx3-SS (C), and Prx3-SOOH (D) to kinetic parameters within the model. These plots order the parameters from greatest to least effect on the model output. The model prediction for $[H_2O_2]$ was most sensitive to k_1, the rate of generation of H_2O_2 by OxPhos, closely followed by the rate constant of oxidation of Prx3-SH, k_6. Prx3-SS was similarly sensitive to k_1 and was also sensitive to k_{10}, the rate constant of reduction of Prx3-SS by Trx2-SH. Prx3-SH was not very sensitive to any single model parameter, and Prx3-SOOH was sensitive to several parameters, especially k_1. k_1 appeared in all four sensitivity analyses as a top parameter, indicating its importance to all the model predictions. The sensitivity analysis, therefore, pointed to the model's overall dependence on the rate of H_2O_2 input into the system and the kinetic parameters within the Trx2/Prx3 pathway.

Once the baseline was established, we next sought to evaluate the network response to H_2O_2 perturbations. To clearly show dynamic behavior during a range of perturbations, we fixed the initial concentration of Prx3-SH at 62 μM, one of the ten concentrations examined in Fig 2 and a value that is close to a previous experimental measurement [35]. The magnitude of the perturbation term, k_{DAAO}, was varied up to 70 μM/s, at which point the reaction network showed evidence of nearing saturation, demonstrated in Fig 4 by changes in the shape of the H_2O_2 traces at high perturbation rates. Fig 4A depicts the concentration of H_2O_2 over time for each perturbation rate simulated. For all but the highest values of k_{DAAO}, the H_2O_2 concentration settled out to a new steady state within milliseconds. It can be observed from the plots of Prx3 dynamics in Fig 4B–4D that this antioxidant pool controls the dynamics of mitochondrial H_2O_2. Prx3-SH concentration reached a new steady state for each perturbation rate, reflecting the predicted H_2O_2 behavior. Prx3-SS concentrations jumped to correspondingly higher levels for each perturbation rate, and in the range of 23–47 μM/s of increased H_2O_2 generation, slowly declined over the 1 hr simulation, accompanied by a slow increase in the Prx3-SOOH isoform. At perturbations above 47 μM/s, the H_2O_2 concentration followed a sigmoid trend that reached an asymptote of tens of μM. This was accompanied by a collapse of the Prx3 network, demonstrated by Fig 4B and 4C. At these very high perturbations, all of the Prx3 became

Table 4. Summary of fractional oxidation of major antioxidants in the network.

Species	Fraction oxidized
Prx3 (dimer)	0.021–0.048
Gpx1	5.4x10-4–1.3x10^{-3}
Prx5 (dimer)	3.6x10-5–8.5x10^{-5}
Gpx4	8.7x10-7–2.1x10^{-6}

https://doi.org/10.1371/journal.pcbi.1008202.t004

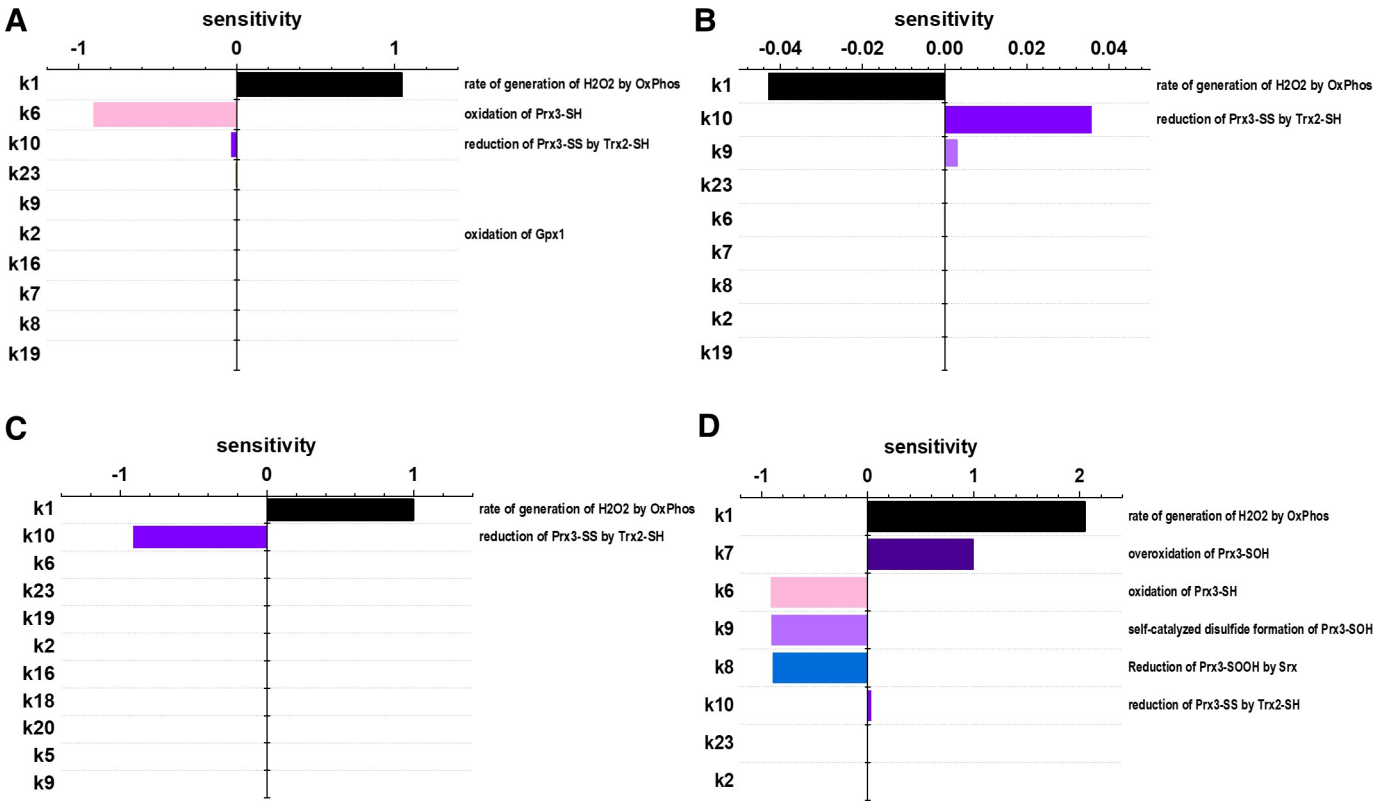

Fig 3. Sensitivity analysis to identify dominant H_2O_2 clearance reactions and assess the impact of uncertainty in parameter values on predicted steady-state basal concentrations. Tornado plots of sensitivities to model rate parameters for A) [H_2O_2], B) [Prx3-SH], C) [Prx3-SS], and D) [Prx3-SOOH] when $k_{DAAO} = 0$. Plots show model rate constants in descending order of sensitivities (absolute value) and are truncated to show only sensitivities above $|10^{-5}|$.

https://doi.org/10.1371/journal.pcbi.1008202.g003

trapped as the hyperoxidized isoform, shown in Fig 4D. It is only when the capacity of the Prx3/Trx/TR system was exceeded that other antioxidants were able to kinetically compete and react with H_2O_2, as summarized by Table 5, which lists the fractional oxidation for the four major antioxidant species at each perturbation rate, following the same convention as in Table 4. It is important to note that the predicted steady states that result from this H_2O_2 perturbation analysis are the net effect of the rate of H_2O_2 generation by OxPhos and the additional k_{DAAO} generation term; a higher OxPhos generation rate would result in a lower k_{DAAO} needed to cause collapse of the Prx3 system.

In order to experimentally investigate the trends predicted by the model, we used the genetically-encoded H_2O_2 generator mito-DAAO, which localizes a H_2O_2 perturbation to the mitochondrial matrix [10,70]. We varied the concentration of D-alanine (D-ala) substrate the cells were exposed to for up to 1 hr, then probed the Prx3 and Prx2 isoforms using redox Western blots. Prx2 is found in the cytosol and provided a means to assess H_2O_2 efflux from the mitochondria to the cytosol. The Western blot results are summarized in Fig 5. The experimental data demonstrates consistently higher fractions of oxidized, dimer Prx3 than the model predicts, and this discrepancy is most prominent at high perturbations. Where the model predicts a maximum fractional oxidation of Prx3 to the disulfide-linked dimer form of around 0.5, the experimental data continues to rise monotonically, reaching a fraction of oxidized Prx3 as high as 0.8. Thus, the model over-predicts hyperoxidation. An increase in the concentration of Prx3 during the perturbation could contribute to a lesser degree of oxidation than expected.

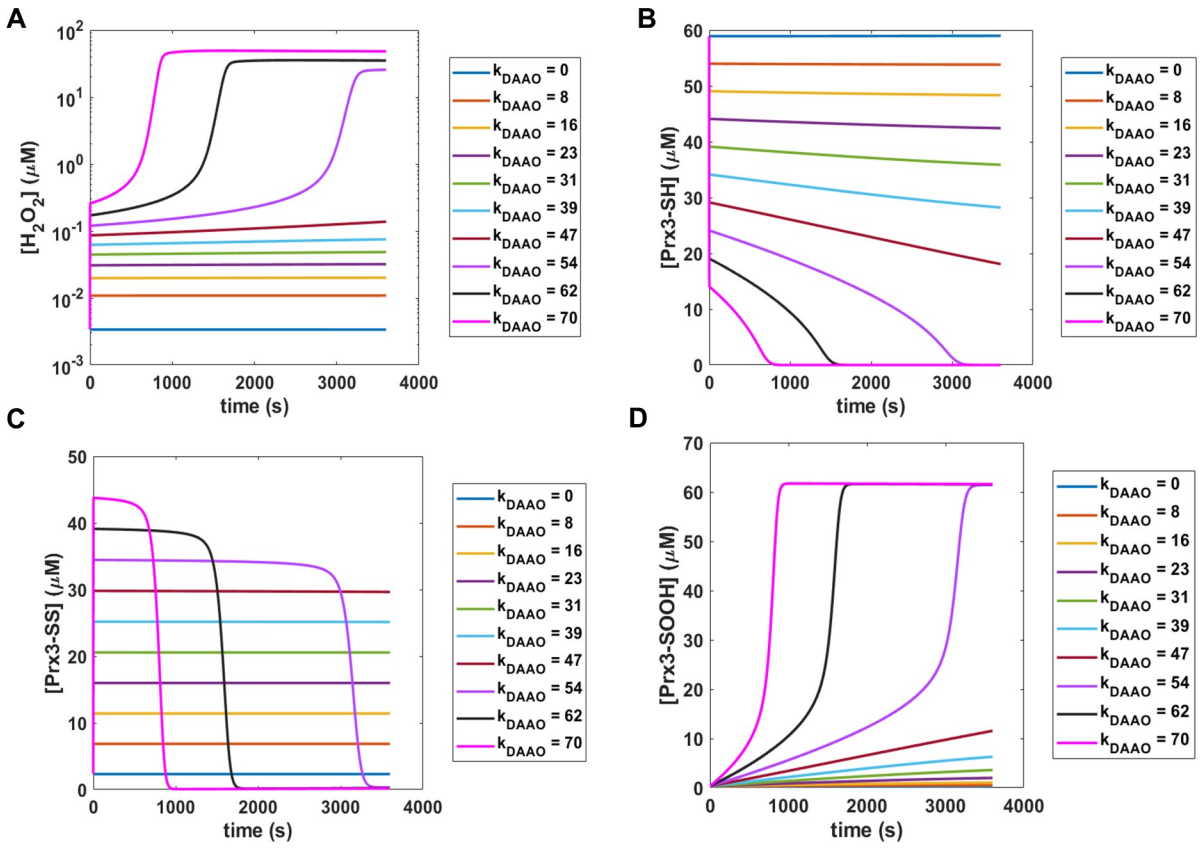

Fig 4. Perturbation analysis. Plots showing the dynamics of A) [H_2O_2], B) [Prx3-SH], C) [Prx3-SS], and D) [Prx3-SOOH] with an initial Prx3-SH concentration of 62 μM for increasing values of k_{DAAO}. All values of k_{DAAO} in μM/s.

https://doi.org/10.1371/journal.pcbi.1008202.g004

We examined whether the total amount of Prx3 increased during increased H_2O_2 generation for up to 1 hour, and found no evidence of increases in total Prx3 abundance (S4 Fig).

The Prx2 data demonstrate increased H_2O_2 flux in the cytosol at certain perturbations after 15 min. At 15 min, while one-way ANOVA testing determined there was a statistically significant trend in Prx3 mean fractional oxidation at the 95% confidence level (P = 0.041), the same

Table 5. Summary of fractional oxidation with changing H_2O_2 perturbations for the major antioxidants in the network at 1 hr with an initial Prx3-SH concentration of 62 μM.

k_{DAAO} (μM/s)	Fraction Oxidized			
	Prx3 (SS dimer)	Gpx1	Prx5 (SS dimer)	Gpx4
0	0.04	$7.68x10^{-4}$	$6.52x10^{-5}$	$1.23x10^{-6}$
8	0.11	$2.47x10^{-3}$	$2.11x10^{-4}$	$3.96x10^{-6}$
16	0.18	$4.56x10^{-3}$	$3.90x10^{-4}$	$7.31x10^{-6}$
23	0.26	0.01	$6.21x10^{-4}$	$1.16x10^{-5}$
31	0.33	0.01	$9.44x10^{-4}$	$1.77x10^{-5}$
39	0.41	0.02	$1.47x10^{-3}$	$2.74x10^{-5}$
47	0.48	0.03	$2.69x10^{-3}$	$5.02x10^{-5}$
54	0.01	0.85	0.25	0.01
62	$3.83x10^{-3}$	0.89	0.29	0.01
70	$2.82x10^{-3}$	0.92	0.33	0.02

https://doi.org/10.1371/journal.pcbi.1008202.t005

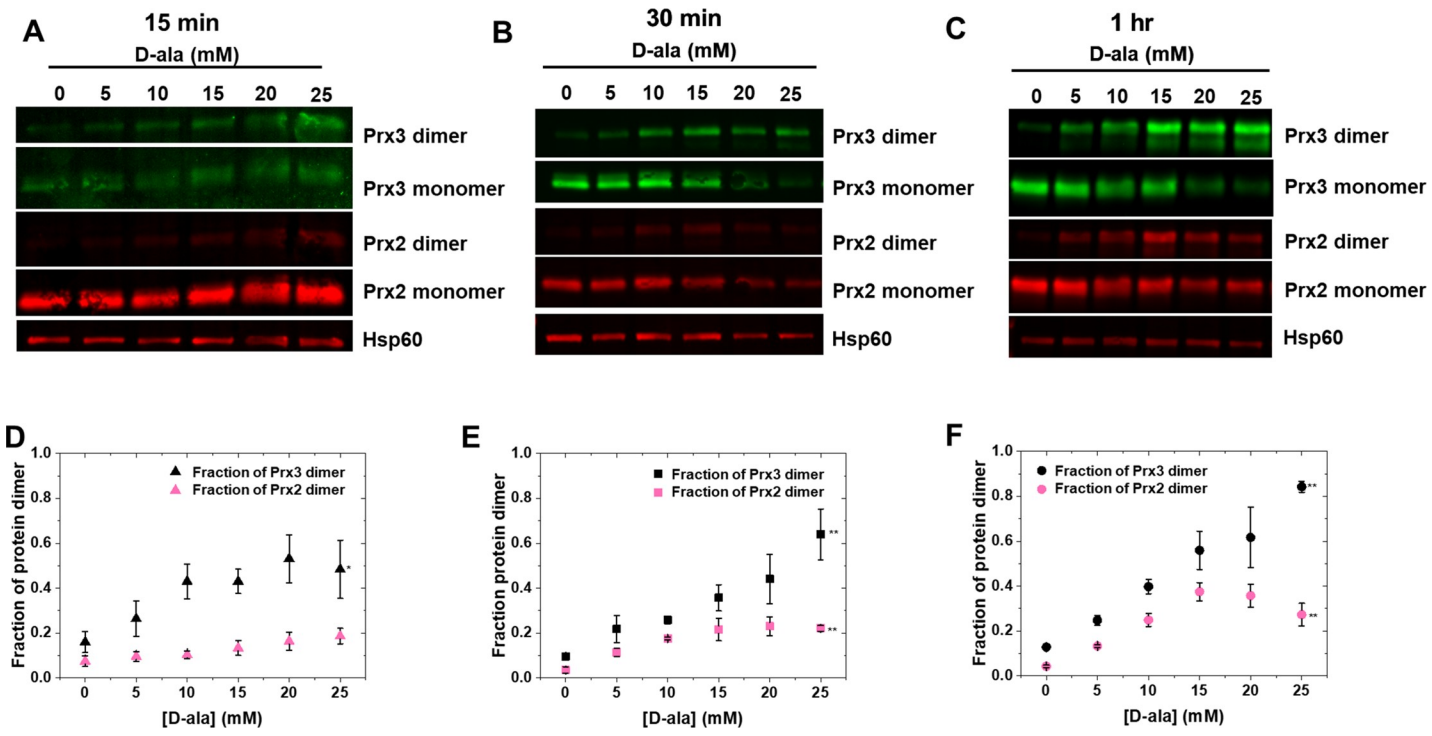

Fig 5. Comparison with experimental data. Western blot analysis of the oxidized (dimer) and reduced (monomer) Prx isoforms after A) 15 min, B) 30 min, and C) 1 hr of H_2O_2 generation by mito-DAAO, with corresponding densitometry plots in D, E, and F, respectively. * represents $P<0.05$ for one-factor ANOVA, ** represents $P<0.01$ for one-factor ANOVA. Full Western blot images can be found in S5–S13 Figs.

https://doi.org/10.1371/journal.pcbi.1008202.g005

test found the Prx2 means to *not* differ across D-ala concentrations ($P = 0.095$) suggesting an undetectable amount of transport at this time scale. However, at subsequent times, both Prx3 and Prx2 oxidation demonstrated significant trends at the 99% confidence level, as determined by one-way ANOVA ($P = 0.004$ and $P = 0.003$ for Prx3 and Prx2 at 30 min, $P = 1.76 \times 10^{-5}$ and $P = 2.05 \times 10^{-5}$ for Prx3 and Prx2 at 1 hr). This suggests that transport effects may be playing a larger role at these longer times, as Prx2 oxidation becomes increasingly significant. This efflux of H_2O_2 from the mitochondria to the cytosol may explain, at least in part, why Prx3 did not collapse into the hyperoxidized form after reaching dimer fractions above 0.5 as predicted by a model that neglects H_2O_2 efflux.

Motivated by this experimental evidence, we refined the kinetic model to include an H_2O_2 efflux reaction that is dependent on the concentration of H_2O_2 as shown in Fig 6A. The range of values of k_{DAAO} where H_2O_2 efflux is substantial and the values of k_{efflux} are both uncertain. Monte Carlo parameter sampling was used to explore ranges of both of these variables. Fig 6 shows the results of sampling high values of k_{DAAO} and comparing two cases: a range of low values of k_{efflux} and a range of high values of k_{efflux}.

When the range of k_{efflux} values is lower than the range of high k_{DAAO} values, including those predicted in Fig 4 to result in collapse of the Prx3 system, Fig 6B shows system behavior that is similar to Fig 4. The concentration of H_2O_2 in mitochondria increases dramatically into the micromolar range as Prx3 becomes completely hyperoxidized (Prx3-SOOH) on the minutes timescale. Sampling k_{efflux} values in the same range as the large k_{DAAO} values that were sampled results in dynamics of the system that are more similar to, though not the same as, the experimental data (S14 Fig). The high k_{efflux} cases in Fig 6B–6F represent a range of values that prevent collapse of the Prx3 system, maintaining H_2O_2 concentrations in the nanomolar range

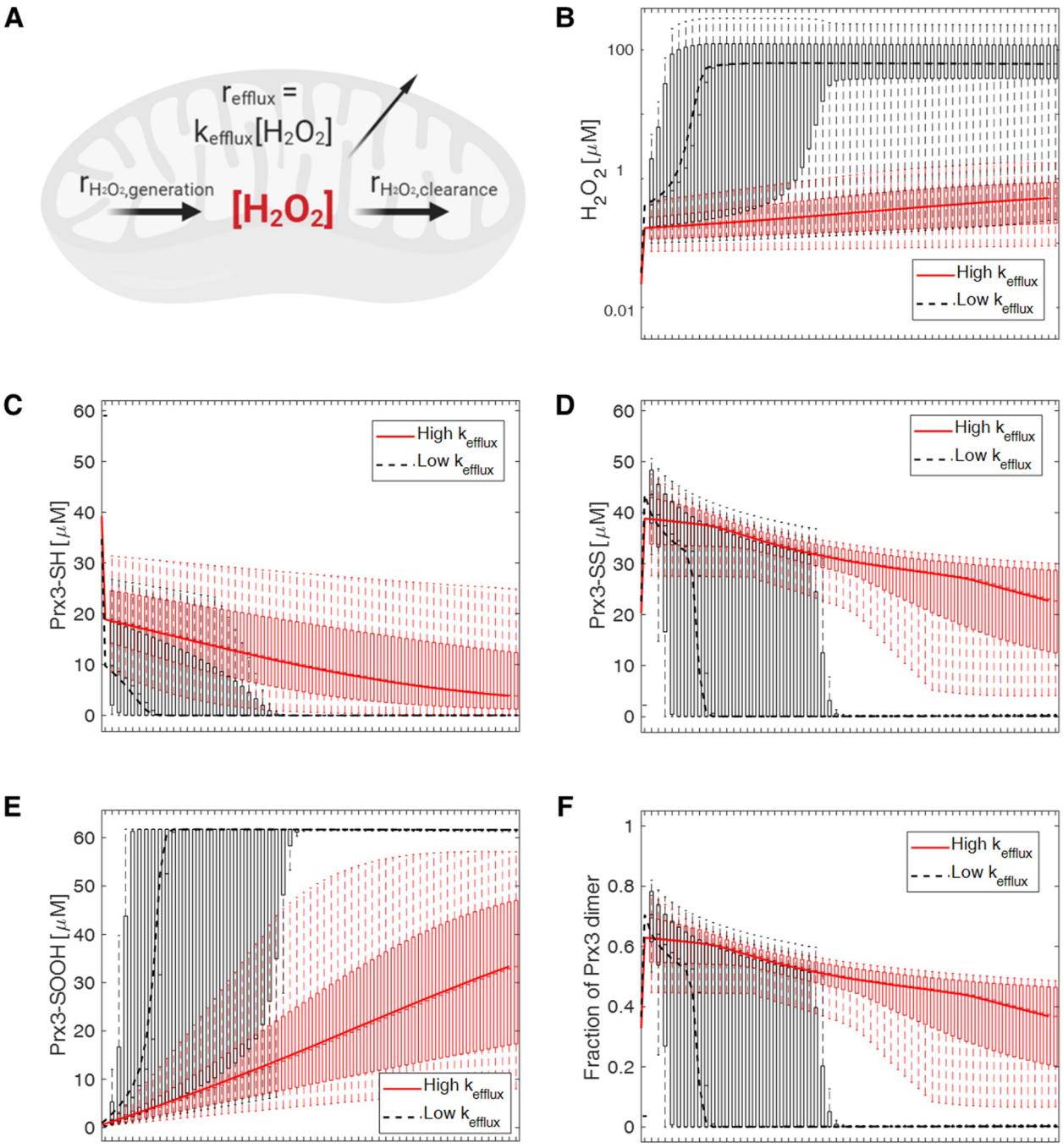

Fig 6. Model refinement and predictions with H_2O_2 efflux rate. A) Schematic of a refined kinetic model that includes the rate of H_2O_2 efflux. B) Model predictions of H_2O_2 dynamics under high production rates of H_2O_2 with either low or high efflux rate. 10,000 samples were randomly generated based on uniform distribution of rates ranging from 50 to 100 μM/s for k_{DAAO}, 0 to 50 μM/s for low k_{efflux} conditions, and 50 to 100 μM/s for high k_{efflux} conditions. Lines represent median values. Points represented in box plot form show 2.5, 25, 75, and 97.5 percentile values at times ranging from 0 to 60 minutes. Dynamic behaviors of Prx3-SH, Prx3-SS, Prx3-SOOH, and the fraction of Prx3 dimer are presented in C), D), E) and F).

https://doi.org/10.1371/journal.pcbi.1008202.g006

and resulting in dimer fractions that are larger than 0.4. This modelling approach still seems to over-predict hyperoxidation.

Discussion

Our analysis of mitochondrial H_2O_2 metabolism found that Prx3 is the antioxidant in the mitochondrial H_2O_2 reaction network that controls the steady state concentration of H_2O_2, as has been previously hypothesized [35]. In HeLa cells, we predicted basal H_2O_2 to be in the range of 2–4 nM. Further, we examined the impact of increasing H_2O_2 generation rates on the reaction network. Because of the reducing capacity of Prx3, the mitochondrial reaction network is able to control H_2O_2 perturbations in the low μM/s range without participation from Gpx1, Prx5, and Gpx4. Only at perturbations that cause total saturation of the Prx3 system do we expect oxidation of Gpx1, Prx5, and Gpx4. Thus, under most circumstances, Prx5 and Gpx4 are not expected to react directly with H_2O_2, consistent with the peer-reviewed literature describing their other roles. It has been previously reported that, though Prx5 and Gpx4 are able to react with H_2O_2, that is not their primary biological function; Prx5 is the putative reductant of reactive nitrogen species and Gpx4 is hypothesized to react with lipid hydroperoxides [23,56,71].

A model that neglects efflux of H_2O_2 from the mitochondria to the cytosol predicts a great deal of hyperoxidation of Prx3 at moderate to large perturbation rates. This is inconsistent with experimental observations of monotonically increasing dimeric Prx3-SS in redox Western blots as a function of increasing H_2O_2 generation rates (Fig 5). If hyperoxidation of Prx3 became prevalent at a particular increased H_2O_2 generation rate, it would be evidenced experimentally by a decrease in the intensity of the dimeric Prx3-SS band. This behavior was observed for Prx2 (Fig 5F). Prx3 is known to be less prone to hyperoxidation as compared with Prx2, as it has faster resolution kinetics of disulfide formation [44,72]. One limitation to accurately predicting Prx3 hyperoxidation is that the reduction kinetics of the sulfinic acid form of Prx3 have not been well characterized, nor the dynamics of Srx import into and export from the mitochondria. In addition, the reduction of Srx itself is still poorly understood [73]. More careful quantitative analyses of the kinetics governing this reaction pathway will improve our understanding of the dynamics of hyperoxidation. However, the largest contributor to the inconsistency of the model's predictions with experimental data at large perturbation rates arises from neglecting efflux. Redox Western blots of mitochondrial and cytosolic Prx isoforms showed that while efflux of H_2O_2 from the mitochondria to the cytosol wasn't detectable at 15 minutes, it became increasing important at longer times over the range of perturbations studied.

Physiologically, a variety of interesting reactions within and across the mitochondrial membranes may occur over the range of perturbation rates we studied, including aquaporin or other pore-mediated diffusion of H_2O_2 into the cytosol and even possible depolarization of the mitochondrial membrane caused by the mitochondrial permeability transition (MPT) [74–76]. The molecular details of these and many other stress responses within mitochondria are not precisely understood. The compartment-specific perturbation tool used here and others that are complementary [77] may provide a means to better understand redox metabolism in this important organelle.

In a study of isolated mitochondria [40], Treberg et al. calculated H_2O_2 consumption rates and estimated steady state mitochondrial H_2O_2 concentrations of $\leq 484 \pm 28$ nM. In our present study of mitochondria within cells, the kinetic model says that the consumption rate of H_2O_2 is expected to be the same at steady-state as the generation rates of H_2O_2 via OxPhos and the DAAO system. With the concentration of Prx3 is taken as 62 μM within mitochondria, we calculated steady-state H_2O_2 concentrations of 3.4–230 nM with a generation rate from OxPhos of 4 μM/s and $0 \leq k_{DAAO} \leq 47$ μM/s. Notably, our range in intact cells, even with extreme k_{DAAO} perturbations, is lower than the upper bound for isolated mitochondria. Our

prediction of basal, steady-state concentrations of 2–4 nM H_2O_2 in the mitochondria of HeLa cells, with the range dependent on Prx3 concentrations from 48–110 μM, is also lower than the previously predicted value of 40 nM [20]. This previous estimate was derived using parameters for a faster respiring cell type, which would produce more H_2O_2 through OxPhos, perhaps leading to higher basal H_2O_2 concentrations. Our findings suggest the utility of measuring Prx oxidation as a marker of H_2O_2 concentrations. Other groups have pointed out that the Prxs could be informative biomarkers for certain cancers [78,79]. This model corroborates that idea, and demonstrates not only a relationship between Prx oxidation and H_2O_2 perturbation, but also Prx oxidation and the total available pool. Moving forward, this model can be used as a general framework for understanding mitochondrial H_2O_2 clearance, and it can be parametrized to match other cells and tissues as data become available.

Supporting information

S1 Appendix. Code, calculations, system of ODEs, further explanations.
(DOCX)

S1 Fig. Baseline H_2O_2 concentration as a function of Prx3 pool for a higher H_2O_2 generation rate by OxPhos (11 μM/s). A value of 4 μM/s was used to generate the figures used in the main text.
(TIF)

S2 Fig. Dimer fraction as a function of Prx3 pool for a higher rate of H_2O_2 generation from OxPhos (11 μM/s). A value of 4 μM/s was used to generate the figures used in the main text.
(TIF)

S3 Fig. Baseline concentrations of reduced and oxidized isoforms of major antioxidant species for a fixed pool of Prx3 (62 μM) and a higher rate of H_2O_2 generation by OxPhos (11 μM/s). A value of 4 μM/s was used to generate the figures used in the main text.
(TIF)

S4 Fig. Additive intensities of all Prx3 bands (reduced and oxidized) as a function of D-ala concentration (0–24 mM) and time of increased H2O2 generation in the mitochondria (15 min.- 1 hr.). Band intensities were normalized to the endogenous protein used as a loading control (Hsp60) and each data point represents an independent replicate.
(TIF)

S5 Fig. Full Western blot image from Fig 5 stained for Prx2 and Hsp60, visualized using IRDye680, showing samples from 15 min of generation, 0–25 mM D-ala (left to right).
(TIF)

S6 Fig. Full Western blot image from Fig 5 stained for Prx3, visualized using IRDye800, showing samples from 15 min of generation, 0–25 mM D-ala (left to right).
(TIF)

S7 Fig. Corresponding stain-free total protein image of 15 min Western blot.
(TIF)

S8 Fig. Full Western blot image from Fig 5 stained for Prx2 and Hsp60, visualized using IRDye680, showing samples from 30 min of generation, 0–25 mM D-ala (left to right).
(TIF)

S9 Fig. Full Western blot image from Fig 5 stained for Prx3, visualized using IRDye800, showing samples from 30 min of generation, 0–25 mM D-ala (left to right).
(TIF)

S10 Fig. Corresponding stain-free total protein image of 30 min Western blot.
(TIF)

S11 Fig. Full Western blot image from Fig 5 stained for Prx2 and Hsp60, visualized using IRDye680, showing samples from 1 hr of generation, 0–25 mM D-ala (left to right).
(TIF)

S12 Fig. Full Western blot image from Fig 5 stained for Prx3, visualized using IRDye800, showing samples from 1 hr of generation, 0–25 mM D-ala (left to right).
(TIF)

S13 Fig. Corresponding stain-free total protein image of 1 hr Western blot.
(TIF)

S14 Fig. Comparison of simulations from Fig 6 with experimental data from Fig 5.
(TIF)

Acknowledgments

The authors thank the lab of R. Ratan at Weill Medical College, White Plains, NY for generously supplying the original mito-DAAO plasmid and William M. Deen for helpful discussion.

Author Contributions

Conceptualization: Kassi T. Stein, Hadley D. Sikes.

Formal analysis: Kassi T. Stein, Sun Jin Moon.

Funding acquisition: Hadley D. Sikes.

Investigation: Kassi T. Stein, Athena N. Nguyen.

Methodology: Kassi T. Stein, Hadley D. Sikes.

Supervision: Hadley D. Sikes.

Writing – original draft: Kassi T. Stein, Hadley D. Sikes.

Writing – review & editing: Kassi T. Stein, Sun Jin Moon, Athena N. Nguyen, Hadley D. Sikes.

References

1. Sies H. Hydrogen peroxide as a central redox signaling molecule in physiological oxidative stress: Oxidative eustress. Redox Biol. 2017; 11: 613–619. https://doi.org/10.1016/j.redox.2016.12.035 PMID: 28110218
2. Angelova PR, Abramov AY. Functional role of mitochondrial reactive oxygen species in physiology. Free Radic Biol Med. 2016; 100: 81–85. https://doi.org/10.1016/j.freeradbiomed.2016.06.005 PMID: 27296839
3. Lennicke C, Rahn J, Lichtenfels R, Wessjohann LA, Seliger B. Hydrogen peroxide–production, fate and role in redox signaling of tumor cells. Cell Commun Signal. 2015; 13: 39. https://doi.org/10.1186/s12964-015-0118-6 PMID: 26369938
4. Fu L, Liu K, Sun M, Tian C, Sun R, Morales Betanzos C, et al. Systematic and Quantitative Assessment of Hydrogen Peroxide Reactivity With Cysteines Across Human Proteomes. Mol Cell Proteomics. 2017; 16: 1815–1828. https://doi.org/10.1074/mcp.RA117.000108 PMID: 28827280

5. Lim JB, Langford TF, Huang BK, Deen WM, Sikes HD. A reaction-diffusion model of cytosolic hydrogen peroxide. Free Radic Biol Med. 2016; 90: 85–90. https://doi.org/10.1016/j.freeradbiomed.2015.11.005 PMID: 26561774

6. Winterbourn CC. Are free radicals involved in thiol-based redox signaling? Free Radic Biol Med. 2015; 80: 164–170. https://doi.org/10.1016/j.freeradbiomed.2014.08.017 PMID: 25277419

7. Mailloux RJ, McBride SL, Harper M-E. Unearthing the secrets of mitochondrial ROS and glutathione in bioenergetics. Trends Biochem Sci. 2013; 38: 592–602. https://doi.org/10.1016/j.tibs.2013.09.001 PMID: 24120033

8. Bak DW, Weerapana E. Cysteine-mediated redox signalling in the mitochondria. Mol Biosyst. 2015; 11: 678–697. https://doi.org/10.1039/c4mb00571f PMID: 25519845

9. Hamanaka RB, Chandel NS. Mitochondrial reactive oxygen species regulate cellular signaling and dictate biological outcomes. Trends Biochem Sci. 2010; 35: 505–513. https://doi.org/10.1016/j.tibs.2010.04.002 PMID: 20430626

10. Stein KT, Moon SJ, Sikes HD. Mitochondrial H_2O_2 Generation Using a Tunable Chemogenetic Tool to Perturb Redox Homeostasis in Human Cells and Induce Cell Death. ACS Synth Biol. 2018; 7: 2037–2044. https://doi.org/10.1021/acssynbio.8b00174 PMID: 30138563

11. Huang BK, Stein KT, Sikes HD. Modulating and Measuring Intracellular H_2O_2 Using Genetically Encoded Tools to Study Its Toxicity to Human Cells. ACS Synth Biol. 2016; https://doi.org/10.1021/acssynbio.6b00120 PMID: 27428287

12. Winterbourn CC. Reconciling the chemistry and biology of reactive oxygen species. Nat Chem Biol. 2008; 4: 278–286. https://doi.org/10.1038/nchembio.85 PMID: 18421291

13. Gauthier LD, Greenstein JL, O'Rourke B, Winslow RL. An Integrated Mitochondrial ROS Production and Scavenging Model: Implications for Heart Failure. Biophys J. 2013; 105: 2832–2842. https://doi.org/10.1016/j.bpj.2013.11.007 PMID: 24359755

14. Kembro JM, Aon MA, Winslow RL, O'Rourke B, Cortassa S. Integrating Mitochondrial Energetics, Redox and ROS Metabolic Networks: A Two-Compartment Model. Biophys J. 2013; 104: 332–343. https://doi.org/10.1016/j.bpj.2012.11.3808 PMID: 23442855

15. Park J, Lee J, Choi C. Mitochondrial Network Determines Intracellular ROS Dynamics and Sensitivity to Oxidative Stress through Switching Inter-Mitochondrial Messengers. PLoS One. 2011; 6: e23211. https://doi.org/10.1371/journal.pone.0023211 PMID: 21829717

16. Wagner BA, Venkataraman S, Buettner GR. The rate of oxygen utilization by cells. Free Radic Biol Med. 2011; 51: 700–712. https://doi.org/10.1016/j.freeradbiomed.2011.05.024 PMID: 21664270

17. Calvo SE, Clauser KR, Mootha VK. MitoCarta2.0: an updated inventory of mammalian mitochondrial proteins. Nucleic Acids Res. 2016; 44: D1251–D1257. https://doi.org/10.1093/nar/gkv1003 PMID: 26450961

18. Hall A, Karplus PA, Poole LB. Typical 2-Cys peroxiredoxins—structures, mechanisms and functions. FEBS J. 2009; 276: 2469–2477. https://doi.org/10.1111/j.1742-4658.2009.06985.x PMID: 19476488

19. Portillo-Ledesma S, Randall LM, Parsonage D, Dalla Rizza J, Karplus PA, Poole LB, et al. Differential Kinetics of Two-Cysteine Peroxiredoxin Disulfide Formation Reveal a Novel Model for Peroxide Sensing. Biochemistry. 2018; 57: 3416–3424. https://doi.org/10.1021/acs.biochem.8b00188 PMID: 29553725

20. Antunes F, Salvador A, Marinho HS, Alves R, Pinto RE. Lipid peroxidation in mitochondrial inner membranes. I. An integrative kinetic model. Free Radic Biol Med. 1996; 21: 917–943. https://doi.org/10.1016/s0891-5849(96)00185-2 PMID: 8937879

21. Pannala VR, Dash RK. Mechanistic characterization of the thioredoxin system in the removal of hydrogen peroxide. Free Radic Biol Med. 2014/10/29. 2015; 78: 42–55. https://doi.org/10.1016/j.freeradbiomed.2014.10.508 PMID: 25451645

22. Lim JB, Huang BK, Deen WM, Sikes HD. Analysis of the lifetime and spatial localization of hydrogen peroxide generated in the cytosol using a reduced kinetic model. Free Radic Biol Med. 2015; 89: 47–53. https://doi.org/10.1016/j.freeradbiomed.2015.07.009 PMID: 26169725

23. Trujillo M, Carballal S, Zeida A, Radi R. Comparative Analysis of Hydrogen Peroxide and Peroxynitrite Reactivity with Thiols. In: Vissers MCM, Hampton MB, Kettle AJ, editors. Hydrogen Peroxide Metabolism in Health and Disease. Boca Raton, FL: CRC Press; 2018. pp. 49–79.

24. Cox AG, Pullar JM, Hughes G, Ledgerwood EC, Hampton MB. Oxidation of mitochondrial peroxiredoxin 3 during the initiation of receptor-mediated apoptosis. Free Radic Biol Med. 2008; 44: 1001–1009. https://doi.org/10.1016/j.freeradbiomed.2007.11.017 PMID: 18164270

25. Trujillo M, Clippe A, Manta B, Ferrer-Sueta G, Smeets A, Declercq J-P, et al. Pre-steady state kinetic characterization of human peroxiredoxin 5: Taking advantage of Trp84 fluorescence increase upon

oxidation. Arch Biochem Biophys. 2007; 467: 95–106. https://doi.org/10.1016/j.abb.2007.08.008 PMID: 17892856

26. Hanschmann E-M, Lönn ME, Schütte LD, Funke M, Godoy JR, Eitner S, et al. Both Thioredoxin 2 and Glutaredoxin 2 Contribute to the Reduction of the Mitochondrial 2-Cys Peroxiredoxin Prx3. J Biol Chem. 2010; 285: 40699–40705. https://doi.org/10.1074/jbc.M110.185827 PMID: 20929858

27. Holmgren A. Thioredoxin structure and mechanism: conformational changes on oxidation of the active-site sulfhydryls to a disulfide. Structure. 1995; 3: 239–243. https://doi.org/10.1016/s0969-2126(01)00153-8 PMID: 7788289

28. Itzhak DN, Tyanova S, Cox J, Borner GHH. Global, quantitative and dynamic mapping of protein subcellular localization. Elife. 2016; 5: 1–36. https://doi.org/10.7554/eLife.16950 PMID: 27278775

29. Mailloux RJ, Craig Ayre D, Christian SL. Induction of mitochondrial reactive oxygen species production by GSH mediated S-glutathionylation of 2-oxoglutarate dehydrogenase. Redox Biol. 2016; 8: 285–297. https://doi.org/10.1016/j.redox.2016.02.002 PMID: 26928132

30. Ghezzi P. Protein glutathionylation in health and disease. Biochim Biophys Acta—Gen Subj. 2013; 1830: 3165–3172. https://doi.org/10.1016/j.bbagen.2013.02.009 PMID: 23416063

31. Beer SM, Taylor ER, Brown SE, Dahm CC, Costa NJ, Runswick MJ, et al. Glutaredoxin 2 Catalyzes the Reversible Oxidation and Glutathionylation of Mitochondrial Membrane Thiol Proteins. J Biol Chem. 2004; 279: 47939–47951. https://doi.org/10.1074/jbc.M408011200 PMID: 15347644

32. Calvo SE, Mootha VK. The Mitochondrial Proteome and Human Disease. Annu Rev Genomics Hum Genet. 2010; 11: 25–44. https://doi.org/10.1146/annurev-genom-082509-141720 PMID: 20690818

33. Noh YH, Baek JY, Jeong W, Rhee SG, Chang T-S. Sulfiredoxin Translocation into Mitochondria Plays a Crucial Role in Reducing Hyperoxidized Peroxiredoxin III. J Biol Chem. 2009; 284: 8470–8477. https://doi.org/10.1074/jbc.M808981200 PMID: 19176523

34. Ribas V, Garci-a-Ruiz C, Fernandez-Checa JC. Glutathione and mitochondria. Front Pharmacol. 2014; 5: 1–19. https://doi.org/10.3389/fphar.2014.00001 PMID: 24478702

35. Cox AG, Winterbourn CC, Hampton MB. Mitochondrial peroxiredoxin involvement in antioxidant defence and redox signalling. Biochem J. 2010; 425: 313–325. https://doi.org/10.1042/BJ20091541 PMID: 20025614

36. Deponte M. Glutathione catalysis and the reaction mechanisms of glutathione-dependent enzymes. Biochim Biophys Acta—Gen Subj. 2013; 1830: 3217–3266. https://doi.org/10.1016/j.bbagen.2012.09.018 PMID: 23036594

37. Holmgren A, Lu J. Thioredoxin and thioredoxin reductase: Current research with special reference to human disease. Biochem Biophys Res Commun. 2010; 396: 120–124. https://doi.org/10.1016/j.bbrc.2010.03.083 PMID: 20494123

38. Chang T-S, Jeong W, Woo HA, Lee SM, Park S, Rhee SG. Characterization of Mammalian Sulfiredoxin and Its Reactivation of Hyperoxidized Peroxiredoxin through Reduction of Cysteine Sulfinic Acid in the Active Site to Cysteine. J Biol Chem. 2004; 279: 50994–51001. https://doi.org/10.1074/jbc.M409482200 PMID: 15448164

39. Chang T-S, Woo HA, Park KJ, Rhee SG, Yang JS, Jeong W, et al. Reduction of Cysteine Sulfinic Acid by Sulfiredoxin Is Specific to 2-Cys Peroxiredoxins. J Biol Chem. 2004; 280: 3125–3128. https://doi.org/10.1074/jbc.C400496200 PMID: 15590625

40. Treberg JR, Munro D, Banh S, Zacharias P, Sotiri E. Differentiating between apparent and actual rates of H2O2 metabolism by isolated rat muscle mitochondria to test a simple model of mitochondria as regulators of H2O2 concentration. Redox Biol. 2015; 5: 216–224. https://doi.org/10.1016/j.redox.2015.05.001 PMID: 26001520

41. Flohé L, Loschen G, Gunzler WA, Eichele E. Glutathione Peroxidase, V. The kinetic mechanism. Hoppe-Seyler's Z Physiol Chem. 1972; 987–999. https://doi.org/10.1515/bchm2.1972.353.1.987 PMID: 5066111

42. Ng CF, Schafer FQ, Buettner GR, Rodgers VGJ. The rate of cellular hydrogen peroxide removal shows dependency on GSH: Mathematical insight into in vivo H 2 O 2 and GPx concentrations. Free Radic Res. 2007; 41: 1201–1211. https://doi.org/10.1080/10715760701625075 PMID: 17886026

43. Yeh GC, Occhipinti SJ, Cowan KH, Chabner BA, Myers CE. Adriamycin Resistance in Human Tumor Cells Associated with Marked Alterations in the Regulation of the Hexose Monophosphate Shunt and Its Response to Oxidant Stress. Cancer Res. 1987; 47: 5994–5999. PMID: 3664503

44. Peskin A V., Dickerhof N, Poynton RA, Paton LN, Pace PE, Hampton MB, et al. Hyperoxidation of Peroxiredoxins 2 and 3. J Biol Chem. 2013; 288: 14170–14177. https://doi.org/10.1074/jbc.M113.460881 PMID: 23543738

45. Antunes F, Brito PM. Quantitative biology of hydrogen peroxide signaling. Redox Biol. 2017; 13: 1–7. https://doi.org/10.1016/j.redox.2017.04.039 PMID: 28528123

46. Sasaki K, Bannai S, Makino N. Kinetics of hydrogen peroxide elimination by human umbilical vein endothelial cells in culture. Biochim Biophys Acta—Gen Subj. 1998; 1380: 275–288. https://doi.org/10.1016/S0304-4165(97)00152-9

47. Huang BK, Sikes HD. Quantifying intracellular hydrogen peroxide perturbations in terms of concentration. Redox Biol. 2014; 2: 955–962. https://doi.org/10.1016/j.redox.2014.08.001 PMID: 25460730

48. Trujillo M, Alvarez B, Radi R. One- and two-electron oxidation of thiols: mechanisms, kinetics and biological fates. Free Radic Res. 2016; 50: 150–171. https://doi.org/10.3109/10715762.2015.1089988 PMID: 26329537

49. Gallogly MM, Mieyal JJ. Mechanisms of reversible protein glutathionylation in redox signaling and oxidative stress. Curr Opin Pharmacol. 2007; 7: 381–391. https://doi.org/10.1016/j.coph.2007.06.003 PMID: 17662654

50. Lo H-W, Antoun GR, Ali-Osman F. The Human Glutathione S -Transferase P1 Protein Is Phosphorylated and Its Metabolic Function Enhanced by the Ser/Thr Protein Kinases, cAMP-Dependent Protein Kinase and Protein Kinase C, in Glioblastoma Cells. Cancer Res. 2004; 64: 9131–9138. https://doi.org/10.1158/0008-5472.CAN-04-0283 PMID: 15604283

51. Johansson C, Lillig CH, Holmgren A. Human Mitochondrial Glutaredoxin Reduces S -Glutathionylated Proteins with High Affinity Accepting Electrons from Either Glutathione or Thioredoxin Reductase. J Biol Chem. 2004; 279: 7537–7543. https://doi.org/10.1074/jbc.M312719200 PMID: 14676218

52. Srinivasan U, Mieyal PA, Mieyal JJ. pH Profiles Indicative of Rate-Limiting Nucleophilic Displacement in Thioltransferase Catalysis. Biochemistry. 1997; 36: 3199–3206. https://doi.org/10.1021/bi962017t PMID: 9115997

53. Henderson GB, Murgolo NJ, Kuriyan J, Osapay K, Kominos D, Berry A, et al. Engineering the substrate specificity of glutathione reductase toward that of trypanothione reduction. Proc Natl Acad Sci. 1991; 88: 8769–8773. https://doi.org/10.1073/pnas.88.19.8769 PMID: 1924337

54. Arnér ESJ, Zhong L, Holmgren A. Preparation and assay of mammalian thioredoxin and thioredoxin reductase. Methods in Enzymology. Academic Press; 1999. pp. 226–239. https://doi.org/10.1016/s0076-6879(99)00129-9 PMID: 9919525

55. Griffith OW, Meister A. Origin and turnover of mitochondrial glutathione (buthionine sulfoximine/y-glutamylcysteine synthetase/y-glutamyl cycle). Proc Natl Acad Sci. 1985; 82: 4668–4672. https://doi.org/10.1073/pnas.82.14.4668 PMID: 3860816

56. Han X, Fan Z, Yu Y, Liu S, Hao Y, Huo R, et al. Expression and characterization of recombinant human phospholipid hydroperoxide glutathione peroxidase. IUBMB Life. 2013; 65: 951–956. https://doi.org/10.1002/iub.1220 PMID: 24170573

57. Kil IS, Ryu KW, Lee SK, Kim JY, Chu SY, Kim JH, et al. Circadian Oscillation of Sulfiredoxin in the Mitochondria. Mol Cell. 2015; 59: 651–663. https://doi.org/10.1016/j.molcel.2015.06.031 PMID: 26236015

58. Milo, R, Philips R. » {How} big are mitochondria? [Internet]. [cited 1 Jun 2018]. Available: http://book.bionumbers.org/how-big-are-mitochondria/

59. Posakony J. Mitochondrial growth and division during the cell cycle in HeLa cells. J Cell Biol. 1977; 74: 468–491. https://doi.org/10.1083/jcb.74.2.468 PMID: 885911

60. Arteel GE, Briviba K, Sies H. Protection against peroxynitrite. FEBS Lett. 1999; 445: 226–230. https://doi.org/10.1016/s0014-5793(99)00073-3 PMID: 10094462

61. Watabe S, Hiroi T, Yamamoto Y, Fujioka Y, Hasegawa H, Yago N, et al. SP-22 is a thioredoxin-dependent peroxide reductase in mitochondria. Eur J Biochem. 1997; 249: 52–60. https://doi.org/10.1111/j.1432-1033.1997.t01-1-00052.x PMID: 9363753

62. Lee MH, Han JH, Lee J-H, Choi HG, Kang C, Kim JS. Mitochondrial Thioredoxin-Responding Off–On Fluorescent Probe. J Am Chem Soc. 2012; 134: 17314–17319. https://doi.org/10.1021/ja308446y PMID: 23017013

63. Adimora NJ, Jones DP, Kemp ML. A Model of Redox Kinetics Implicates the Thiol Proteome in Cellular Hydrogen Peroxide Responses. Antioxid Redox Signal. 2010; 13: 731–743. https://doi.org/10.1089/ars.2009.2968 PMID: 20121341

64. Martinovich GG, Cherenkevich SN, Sauer H. Intracellular redox state: towards quantitative description. Eur Biophys J. 2005; 34: 937–942. https://doi.org/10.1007/s00249-005-0470-3 PMID: 16215752

65. Schafer FQ, Buettner GR. Redox environment of the cell as viewed through the redox state of the glutathione disulfide/glutathione couple. Free Radic Biol Med. 2001; 30: 1191–1212. https://doi.org/10.1016/s0891-5849(01)00480-4 PMID: 11368918

66. Price ND, Schellenberger J, Palsson BO. Uniform sampling of steady-state flux spaces: Means to design experiments and to interpret enzymopathies. Biophys J. 2004; 87: 2172–2186. https://doi.org/10.1529/biophysj.104.043000 PMID: 15454420

67. Yue H, Brown M, Knowles J, Wang H, Broomhead DS, Kell DB. Insights into the behaviour of systems biology models from dynamic sensitivity and identifiability analysis: a case study of an NF-κB signalling pathway. Mol BioSyst. 2006; 2: 640–649. https://doi.org/10.1039/b609442b PMID: 17216045

68. Cox AG, Winterbourn CC, Hampton MB. Measuring the Redox State of Cellular Peroxiredoxins by Immunoblotting. Methods in enzymology. 2010. pp. 51–66. https://doi.org/10.1016/S0076-6879(10)74004-0

69. Powers JF, Cochran B, Baleja JD, Sikes HD, Zhang X, Lomakin I, et al. A unique model for SDH-deficient GIST: an endocrine-related cancer. Endocr Relat Cancer. 2018; 25: 943–954. https://doi.org/10.1530/ERC-18-0115 PMID: 29967109

70. Alim I, Haskew-Layton RE, Aleyasin H, Guo H, Ratan RR. Spatial, Temporal, and Quantitative Manipulation of Intracellular Hydrogen Peroxide in Cultured Cells. Methods Enzymology. 2014. pp. 251–273. https://doi.org/10.1016/B978-0-12-801415-8.00014-X PMID: 25416362

71. Yang WS, SriRamaratnam R, Welsch ME, Shimada K, Skouta R, Viswanathan VS, et al. Regulation of Ferroptotic Cancer Cell Death by GPX4. Cell. 2014; 156: 317–331. https://doi.org/10.1016/j.cell.2013.12.010 PMID: 24439385

72. Cox AG, Pearson AG, Pullar JM, Jönsson TJ, Lowther WT, Winterbourn CC, et al. Mitochondrial peroxiredoxin 3 is more resilient to hyperoxidation than cytoplasmic peroxiredoxins. Biochem J. 2009; 421: 51–58. https://doi.org/10.1042/BJ20090242 PMID: 19356151

73. Lowther WT, Haynes AC. Reduction of Cysteine Sulfinic Acid in Eukaryotic, Typical 2-Cys Peroxiredoxins by Sulfiredoxin. Antioxid Redox Signal. 2011; 15: 99–109. https://doi.org/10.1089/ars.2010.3564 PMID: 20712415

74. Halestrap AP, Clarke SJ, Javadov SA. Mitochondrial permeability transition pore opening during myocardial reperfusion—a target for cardioprotection. Cardiovasc Res. 2004; 61: 372–385. https://doi.org/10.1016/S0008-6363(03)00533-9 PMID: 14962470

75. Hansson MJ, Månsson R, Morota S, Uchino H, Kallur T, Sumi T, et al. Calcium-induced generation of reactive oxygen species in brain mitochondria is mediated by permeability transition. Free Radic Biol Med. 2008; 45: 284–294. https://doi.org/10.1016/j.freeradbiomed.2008.04.021 PMID: 18466779

76. Marchissio MJ, Francés DEA, Carnovale CE, Marinelli RA. Mitochondrial aquaporin-8 knockdown in human hepatoma HepG2 cells causes ROS-induced mitochondrial depolarization and loss of viability. Toxicol Appl Pharmacol. 2012; 264: 246–254. https://doi.org/10.1016/j.taap.2012.08.005 PMID: 22910329

77. Sies H, Reichert AS. Selectively Addressing Mitochondrial Glutathione and Thioredoxin Redox Systems. Cell Chem Biol. 2019; 26: 316–318. https://doi.org/10.1016/j.chembiol.2019.02.017 PMID: 30901559

78. Fischer J, Eglinton T, Frizelle F, Hampton M. Peroxiredoxins in Colorectal Cancer: Predictive Biomarkers of Radiation Response and Therapeutic Targets to Increase Radiation Sensitivity? Antioxidants. 2018; 7: 136. https://doi.org/10.3390/antiox7100136 PMID: 30301137

79. Poynton RA, Hampton MB. Peroxiredoxins as biomarkers of oxidative stress. Biochim Biophys Acta—Gen Subj. 2014; 1840: 906–912. https://doi.org/10.1016/j.bbagen.2013.08.001 PMID: 23939310